archives
of thermodynamics
Vol. **42**(2021), No. 3, 87–113
DOI: 10.24425/ather.2021.138111

Computational fluid dynamics simulation of heat transfer from densely packed gold nanoparticles to isotropic media

PIOTR RADOMSKI[a]*
PAWEŁ ZIÓŁKOWSKI[a]
LUCIANO DE SIO[b]
DARIUSZ MIKIELEWICZ[a]

[a] Gdańsk University of Technology, Faculty of Mechanical Engineering and Shipbuilding, Energy Institute, Narutowicza 11/12, 80-233 Gdańsk, Poland

[b] Sapienza University of Rome, Department of Medico-Surgical Sciences and Biotechnologies, Center for Biophotonics, Piazzale Aldo Moro 5, 00185 Roma, RM, Italy

Abstract This work aims to determine and compare heat generation and propagation of densely packed gold nanoparticles (Au NPs) induced by a resonant laser beam (532 nm) according to the Mie theory. The heat flux propagation is transferred into the materials, which here are: silica glass; soda-lime-silica glass; borosilicate glass; polymethyl methacrylate (PMMA); polycarbonate (PC); and polydimetylosiloxane (PDMS). This analysis aims to select the optimum material serving as a base for using photo-thermo-ablation. On the other hand, research focused only on Newtonian heat transfer in gold, not on non-Fourier ones, like the Cattaneo approach. As a simulation tool, a computational fluid dynamics code with the second-order upwind algorithm is selected. Results reveal a near-Gaussian and Gaussian temperature distribution profile during the heating and cooling processes, respectively. Dependence between the maximum temperature after irradiation and the glass thermal conductivity is observed confirming the Fourier law. Due to the maximum heating area, the borosilicate or soda-lime glass, which serves as a base, shall represent an excellent candidate for future experiments.

*Corresponding Author. Email: piotr.radomski@pg.edu.pl

Keywords: Heat transfer; Gold nanoparticles; Glasses; Polymers; Computational fluid dynamics

Nomenclature

A	–	area of irradiation, m^2
c_p	–	specific heat capacity, J/kgK
$c_{\rho S}$	–	specific heat capacity at a boundary surface, J/kgK
e	–	specific energy, J/kg
h	–	heat transfer coefficient, $W/m^2\,K$
$\vec{F}_{heat}$	–	heat flux
$\vec{F}_{mech}$	–	mechanical forces
I_o	–	incident intensity radiation, W/m
$\overleftrightarrow{I}$	–	Gibss's idemfactor
$\overleftrightarrow{I}_s$	–	Gibss's idemfactor in reference to a surface
k	–	thermal conductivity coefficient, W/m^2K
k_s	–	thermal conductivity coefficient of a surface, W/m^2K
l_{gold}	–	thickness of a gold film, m
l_T	–	Smoluchowski length connected with phenomena and materials, m
l_T^f	–	discontinuity of temperature at fluid part, m
l_T^s	–	discontinuity of temperature at solid part, m
n	–	refractive index
$\vec{n}$	–	normal vector
P_L	–	power of laser, W
$\vec{q}$	–	Fourier heat flux
R_o	–	reflectivity in room temperature
S_e	–	heat generation rate, W/m^3
T	–	temperature, K
T_o	–	reference temperature (= 24°C (297.15 K))
T_S	–	Smoluchowski temperature jump, K
T_{wall}	–	wall temperature, K
t	–	time, s
$\vec{v}_S$	–	surface velocity vector
$\vec{v}_{slip}^f$	–	slip velocity vector in fluid
$\vec{v}_{slip}^s$	–	slip velocity vector in solid

Greek symbols

α	–	incident angle, rad
α_d	–	thermal diffusivity, m^2/s
η	–	efficiency of laser
λ	–	wavelength of incident radiation, m
ξ	–	amount of Au NPs per volume ($= 3.0\times10^{22}\ m^{-3}$)
ρ	–	density, kg/m^3
ρ_S	–	density at a boundary surface, kg/m^3
σ_{abs_o}	–	absorption coefficient in room temperature, m^{-1}

Subscripts and superscripts

abs	–	absorption
ext	–	extinction
heat	–	related to thermodynamics
heat	–	related to thermodynamics
mech	–	related to mechanics
mech	–	related to mechanics
f	–	fluid
s	–	solid
slip	–	related to slip velocity
wall	–	conditions at a wall
o	–	at standard conditions (24°C, 101325 Pa)

Abbreviations

Au	–	gold
CFD	–	computational fluid dynamics
CPU	–	central processing unit
LSPR	–	localized surface plasmon resonance
FEM	–	finite element methods
NP	–	nanoparticle

1 Introduction

1.1 Motivation

Among many publications concerning the simulation of nanoparticles only few consider gold nanoparticles with a computational fluid dynamics (CFD) code, and moreover refer to microfluidic systems or charge transport [1]. Heat transfer and laser interaction have not been published in the reference to gold nanoparticles (Au NPs) using continuum mechanics. Although this work has examined simple and well-known materials, the obtained results might be extended into all isotropic media, regardless if it possesses an organic or inorganic structure.

Firstly, it is worth emphasizing that the "densely packed gold nanoparticles" expression concerns their occupation on a selected area. Secondly, the Au NPs are deposited and embedded on a slab in such a way that they are separated from one another. On the other hand, the distance appears to enable the assumption of inclusions in the slab. In this work, the thickness of the plate was established at 20 nm.

Nevertheless, the main goal is to select the optimum material that might serve as a base for Au NPs. The present topic has not been investigated yet

and this work has been to constitute a curious numerical instance that may be extended to a real experiment based on laser ablation. The next goal of this work is to study by continuum methods (FEM or CFD), the heat transfer in selected isotropic materials (glasses and polymers) as a result of localized surface plasmon resonance (LSPR) phenomenon. The paper also shows that in order to prevent multiscale problems, nanoparticles, not only Au NPs, may be simulated without including their real size in the field of geometry but only by using appropriate material properties and boundary conditions.

The surrounding media might be even expanded on biological media (e.g., human tissues, bio-polymers, skin), which mostly are isotropic as well [2–4, 12]. Thus, another aim is to investigate, which properties should possess the medium so as to achieve the highest temperature and cause the death of bacteria, viruses or even tumors. The maximum temperature at which the tumors overheat is approximately equaled 42°C [39]. However, it is necessary to bear in mind this is the maximum temperature at which the human body keeps metabolic processes. The assumption of properties constancy could also turn out to be legitimate and depend on temperature and, which is much more difficult to simulate, ageing processes dramatically.

1.2 Outline of the work

Gold has been one of the most appreciated materials in the human history. However, in ancient ages, unlike the glass, possession of gold or a gold-decorated vessel was a sign of luxury and membership to the highly-developed elites. In the subsequent ages, the pursuit of gold possession did not undergo severe changes, and many of the scientists were still attempting with a negative effect to achieve pure gold in simple reactions. The perception has kept up nowadays although there are a lot of more valuable and precious materials. As new branches of physics and chemistry, nanoscience and nanotechnology specify the material by their surface modification, which improves most properties (despite superconductivity). It is noticeable with the increasing surface to a volume force ratio, often by the density modification [5, 6].

Noble metals, like gold, are the most stable metals as a bulk compared to the rest of known materials, and only powerful acids could slightly modify their surface. For this reason, their properties change at the nanoscale and it is necessary to specify them from the thermal, structural, and electromagnetic point of view [5, 6]. In the last branch, there is a highly probable phenomenon to apply in heat production. The approach relies on the use

of the localized surface plasmon resonance (LSPR), which produces different energy types, especially heat from electromagnetic waves. The leading theory that describes a photon interaction behavior with metallic nanoparticles (NPs), e.g., silver or gold, is the Gustav Mie theory [4]. It assumes that discrete nanoparticles produce the plasmons which may resonate with the incident electromagnetic wave and may be absorbed effectively. It means all refractive part of light will transfer and produce heat. At first sight, it could seem like a loss of energy. Still, it has a positive character in biological applications because this increase in the human body's temperature triggers an overheat and tumor termination [7–11].

Considering Mie's equations thoroughly, it can be noticed the scattering and absorption coefficients may be represented by Riccati–Bessel functions, which are responsible mainly for the wavelength dependence due to the shape and size of NPs. It provokes many applications in experimental research, but it is a sore place for the calculation methods because of the source heat production dependence. Therefore the continuum methods appear not to be the most appropriate to solve the problems. Nevertheless, after nearly 100 years of the Mie theory's existence, there have been appeared many papers that approximate or substitute this interaction [13–15], and even without using Riccati–Bessel functions in which the extinction coefficient, C_{ext}, is dependent on permittivity of a surrounding medium [7,14]. Hence, the reproduced conditions can differ in suspension, water, milk, human blood, etc., for the Au NPs. Furthermore, the heat transfer in different materials is determined by its thermal properties. The approach, however, requires treating the gold nanoparticles as extrusions in a thin slab, and there are still some limitations that should be considered. It is worth specifying the following issues:

- The interaction between light and NPs can be treated in an indirect form, i.e., only as a source term. It is the simplest method and entirely accurate but does not include the explicit laser beam presence. However, it is sufficient for thermodynamic investigations.

- NPs often occupy space on glasses and are remote from each other that there is a distance between them. It is hard to model such a situation because of their nanosize.

- The absorption and scattering coefficients are highly dependent on the nanostructure of nanoparticles. Regulation of properties by these parameters lets us realize that all the energy may be converted if the NPs are very pure and have an ideal spherical shape. For the

nanoshells, nanorods, or clusters, the energy conversion efficiency will be strongly connected with their geometry [8, 16, 17]. It should also be taken into account the blue- or red-shift phenomenon, which could change the absorption and reflectivity coefficient significantly.

These problems conclude that it is highly improbable to apply the gold nanoparticles (Au NPs) in something different from the sensors and heat production. for the high-quality simulations it requires a high CPU time and memory space. Although plasmon resonance requires a use of quanta mechanics methods the considered problem in terms of time and memory space, the heat transfer provides an opportunity as an aftermath of LSPR phenomenon to evade this rule, and allows to use CFD techniques.

2 Methods

2.1 Governing equations

Based on the Mie theory, it may be supposed that virtually all absorbed energy would be converted to heat released by Au NPs. However, the irradiated area could not respond to the real nanoparticles arrangement. The remaining photons of the beam that could not participate in heat transfer would be reflected, transmitted from the surface or absorbed by the glass as well. Moreover, if there is some distance between Au NPs as spheres, the laser beam shall irradiate merely the part of the surface which occupies the Au NPs. Hence, it may be assumed that only part of the initial energy is able to produce the heat from Au NPs effectively.

There are various computational techniques for the simulation of electromagnetic interaction between two bodies. For instance, discrete ordinates (DO) model allows to calculate the intensity distribution in media including absorption, scattering and transmission phenomena [40–42]. However, in the carried out simulations, the laser beam was not set up as a real part due to several reasons. Firstly, radiation models require much more CPU time and memory. Secondly, this influence as a temperature distribution might be considered as a percentage of source of electromagnetic energy (heat generation rate, S_e), which can be expanded by appropriate boundary conditions. In the applied continuum methods, the gold plate was treated by using the energy equation. It might be described in a simplified formula

$$\frac{\partial}{\partial t}(\rho\, e) = \operatorname{div}(k \operatorname{grad} T) + S_e\,, \tag{1}$$

where: ρ – density of a material, $e = c_p T$ – specific energy, k – thermal conductivity coefficient, T – temperature of the considered body, S_e – source of energy (heat generation rate).

Since the considered system consists of only solids which are not under high stresses, it may be assumed that heat transfer is the same, regardless if it is a boundary or the interior of a cell. Moreover, it is not necessary to specify the mass and momentum balance equations. However, taking into account the micro- and nanoscale effect, the models in which the phase boundary effects are the leading role shall be considered. Such a situation could be invesitgated on the gold–glass or even nanoparticles – blood boundaries. They are based on the widely common case for fluid–solid or solid–solid, if one of them undergoes a local melting or plasticization. For instance, an increase of the mass flow rate in a microchannel can occur due to the arising pressure gradient and connected with rarefication and adhesion of velocity at the boundary [18, 43]. Then the zero-velocity condition is not satisfied and at a non-zero velocity of fluid in this place is found. Usually, it moves in the same direction but there are some exceptions. In any case, the real cost is frequently unviable than the standard, no-slip model [19]. Taking into consideration the rarefied gas model introduced by Maxwell, Coulomb and Darcy it is likely to express the classical kinetic theory of gases with boundary modifications [20]. Maxwell, starting with the Taylor series, expands the theory of gases with derivatives by velocities. The so-defined condition requires to express the stress tensor again [21]. This is the reason why the molecular dynamics, lattice Boltzmann methods or direct simulation Monte Carlo are not appropriate for such simulations. Furthermore, the scale problem and related computational costs reduce possibilities to simulate because of huge multi-core computer workstations. Here continuum methods are the lion's share of the theoretical results. For example, in [21–26] there are presented results of rarefied gases phenomena which seem to formulate such a boundary condition so as to enable using it at a wide range of applications. It is recommended to consider transpiration effects as well but separately pressure, thermal and Graham transpiration.

In spite of all the phenomena, it is worth considering the temperature discontinuities and concentration of chemical components in the normal direction to the wall [27,43]. The temperature jump with discontinuity is not the same as the thermal transpiration which is only a reason to increase the flow transport in a direction. For instance, the Smoluchowski temperature jump is connected with the ambiguity of wall and fluid temperature in this region (Fig. 1).

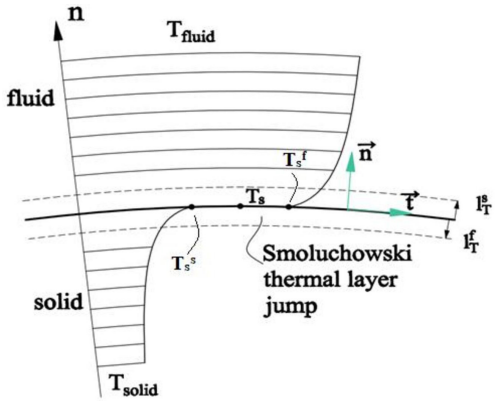

Figure 1: Discontinuity of temperature T_S at fluid l_T^f – solid l_T^s region with including Smoluchowski jump and without it [26].

Suggested by Smoluchowski in 1896 model assumes that temperature jump, expressed by a jump length l_T^f or l_T^s, is bounded according to Stokes's heat law in the following equations [27, 28]:

$$h\left(T - T_{wall}\right) + \vec{q} \cdot \vec{n} = 0, \tag{2}$$

$$\vec{q} = k \operatorname{grad} T, \tag{3}$$

where: h – heat transfer coefficient; T_{wall} – wall temperature; $\vec{q}$ – Fourier heat flux; $\vec{n}$ – normal vector.

Then the Smoluchowski temperature jump length can be expressed by

$$l_T = l_T^s + l_T^f = \frac{k}{\alpha_d}, \tag{4}$$

where: l_T^s – discontinuity of temperature at solid part, l_T^f – discontinuity of temperature at fluid part, α_d – thermal diffusivity.

Therefore, a generalized boundary condition ought to be considered as a surface energy contribution as well as the thermal jump phenomena. Without going into details, let $e_s = c_{\rho s} T_s$ be the simplest form of surface internal energy governed by surface temperature, T_s. Defining the surface metric tensor to be $\overleftrightarrow{I}_S = \overleftrightarrow{I} - \vec{n} \otimes \vec{n}$ (tensor product), and the surface gradient, grad_s, and divergence operator, div_s [21], we are able to express the boundary condition for energy equation within a thermal contact layer. Removing from the balance other energy fluxes and keeping only mechanical,

$\vec{F}_{mech}$, and thermal, $\vec{F}_{heat} \equiv \vec{q}$, vectors on the boundary the energy balance within the thermal contact layer can be written to be

$$\frac{\partial}{\partial t}\left(\rho_S c_{\rho S} T_S\right) + \mathrm{div}_S\left(\rho_S c_{\rho S} T_S \overleftrightarrow{I}_S \vec{v}_S\right) + \mathrm{div}_S\left(k_S \,\mathrm{grad}\, T_S\right) + l_T^f\left(T_S^f - T_S\right) - l_T^s\left(T_S^s - T_S\right) + \alpha_d^f\left(T^f - T_S^f\right) - \alpha_d^s\left(T^s - T_S^s\right) + \left(\vec{q}^f - \vec{q}^s\right)\cdot\vec{n} + \left(\vec{F}_{mech}^f \times \vec{v}_{slip}^f - \vec{F}_{mech}^s \times \vec{v}_{slip}^s\right)\cdot\vec{n} = S_e\,, \tag{5}$$

where in the thermal contact layer an additional surface density, ρ_s, and the surface temperature, T_s, appears with thermal conductivity coefficient of the layer, k_s, and surface specific heat capacity, c_{ps}. The surface velocity vector, $\vec{v}_s$, and the slip velocity vectors, $\vec{v}_{slip}^s$ and $\vec{v}_{slip}^f$, should be independently calculated from the boundary conditions for the momenta equations. The transfer coefficients, α_d^f and α_d^s are responsible for overall transport of thermal energy in the macroscopic vicinity of the contact layer. The Smoluchowski jump coefficients are related to the thermal jump length as $l^f = l_T^f/k_f$ and $l^s = l_T^s/k_s$. This last contribution to equation is especially important in micro- and nanoscales where the mechanism of the Smoluchowski thermal jump becomes most valid. Also, in the nanoscale the energetic contribution from the mechanical slip – for instance the Navier slip – gives the considerable values.

Although the approach appears to be the most suitable tool to simulate, there are a few drawbacks that seem to be unavoidable. The first one is associated with the real shape of atoms and porosity. Continuum methods treat materials as dense and quadratic bodies, which does not reflect the position of atoms. It is not worth concerning it at the macroscale, because the effects are negligible. The situation changes at the micro- and nanoscale, where the surface shapes and forces shall be taken into account. On the other hand, the multiscale difficulties are the issues, which concern many theorists, and although there are many publications of the considered problem like in [29–32], the combination of nano-, micro- and macroscale from 10 nm to 1 cm has become one of the challenges of the theoretical physics. For instance, because of so-called "near-wall" problems, the coupling at fluid-solid boundary in the microscale may not provide sought accuracy while such methods are performed. Furthermore, the techniques appear to be inappropriate for flows with such a geometry in which one dimension is significantly larger than the others [29].

Therefore, in the considering simulations the gold nanoparticles have been simulated as sort of as a "porous" thin film with a thickness l_{gold} equaled 20 nm. The word "porous", however, does not refer to a porous zone strictly, which would require much more CPU time, but as discrete and separated nanoparticles embedded on the wall. Having applied such an approach, it is possible to obey the need of use the mentioned problems under the condition that the heat distributes only inside the materials, not on the gold plate.

2.2 Geometry and discretizetion of space

To present the future experiment system and its conditions, an appropriate geometry has been created. Three main areas have been considered (Fig. 2). The specific dimensions of each area have also been introduced. The largest region, namely the "base", which is an isotropic medium with a 70 mm × 25 mm surface area and 10 mm of thickness, was covered with an isolation at the top wall. The Au NPs, however, were embedded on the center part of base with a 5 mm × 5 mm surface area, and incorporated in the fluid chamber (here is treated as air (isolator), however in the future experiment it can be biological material). It is essential that this part is not taken into account in results, although the calculations included it as well.

A mesh was also prepared for discretization. To reduce the skewness which could lead to problems on edges of a body the rectangular shape (cuboid) was used. The reading data areas (the 5 mm × 5 mm gold plate and X, Y, Z axes) and the mesh and boundary conditions were presented in Fig. 2, whereas all essential information about the implemented mesh has been outlined in Table 1.

Table 1: General information about the considered mesh and the numerical method.

Parameter	Value
Number of nodes	40 1931
Number of bodies	385 000
Mean cell volume	0.653 mm^3
Mean element size	0.5 mm
Residual convergence of energy equation	10^{-6}
Method of energy equation solution	Second order upwind
Mass and momentum balance	Converged but not solved in terms of solids

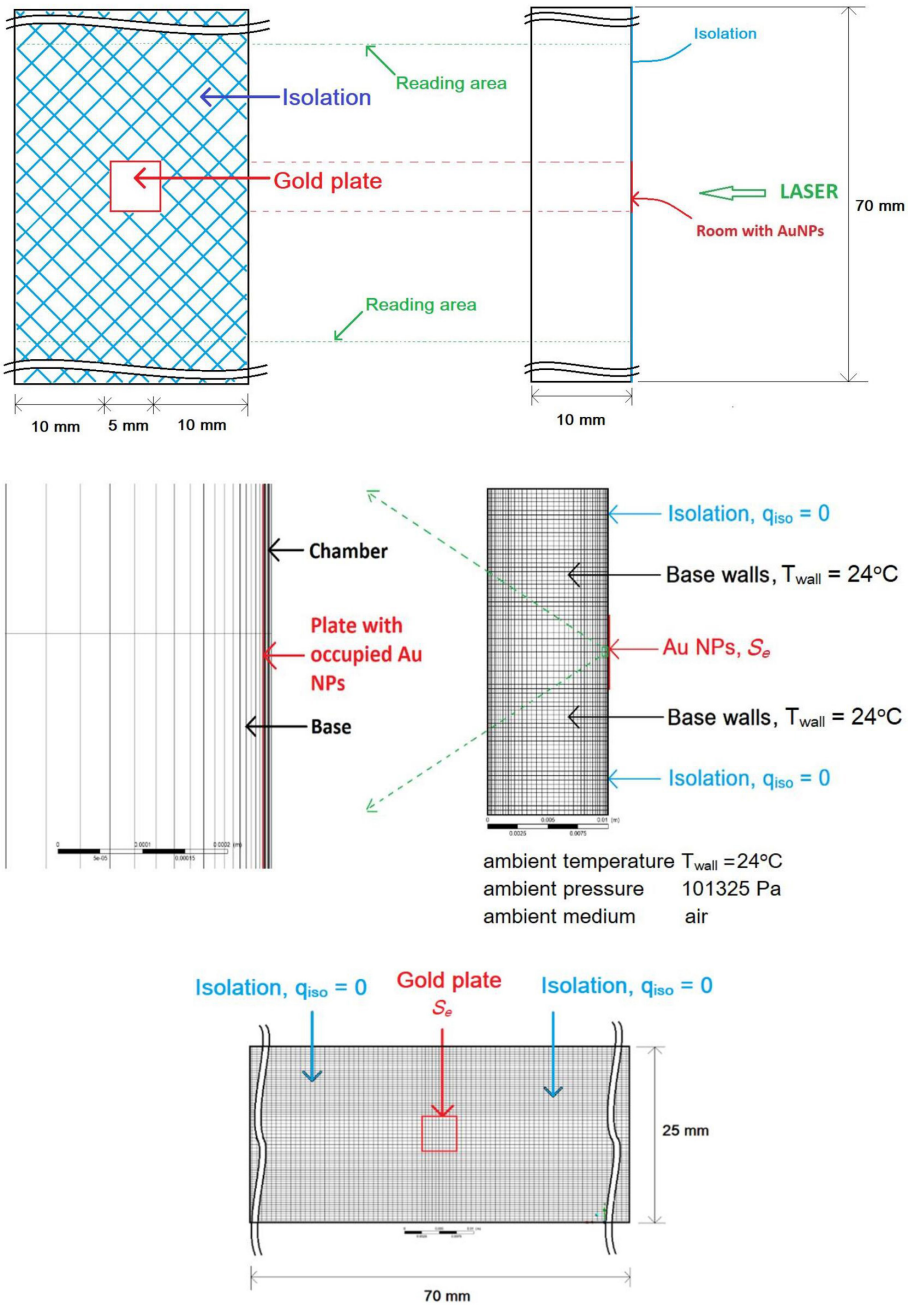

Figure 2: Created geometry (top), and mesh (center) side view with a magnification 500 times and (bottom) at top view for the considered calculations with boundary conditions.

2.3 Material properties

In accomplished simulations there were used values for the pure gold. It is commonly known, however, that the smaller the size of gold nanoparticles (Au NPs), the higher the influence of surface energy over the volume. Bearing that in mind, clear changes at the thermal and mechanical properties might be observed and the results can differ from the experimental ones. It is necessary to remember the size effect and its influence on most properties, especially thermal properties. Then the thermal conductivity coefficient, k, may be less than that of a bulk material and may reach even 100 $\mathrm{Wm^{-1}K^{-1}}$. However, the preliminary simulations revealed virtually no difference in terms of these thermal properties. Therefore, the following parameters were used as constant values at the carried out simulations [33]:

density of gold, $\rho = 19320\ \mathrm{kg\,m^{-3}}$,

specific heat capacity, $c_p = 129.81\ \mathrm{Jkg^{-1}K^{-1}}$,

thermal conductivity coefficient, $k = 317\ \mathrm{Wm^{-1}K^{-1}}$.

For the other type of glass these values can differ and depend on temperature but in this work they have been assumed as constants. Several examples among the most usable glasses in industry and science have been investigated. Its thermal properties are written in Table 2.

Table 2: General thermal properties of materials used in the calculations at 20°C [34–37].

Type of glass	Density, $\mathrm{kg\,m^{-3}}$	Thermal conductivity, $\mathrm{Wm^{-1}K^{-1}}$	Specific heat capacity, $\mathrm{J\,kg^{-1}K^{-1}}$
Inorganic glasses			
Silica glass	2200.0	0.28000	840.00
Soda-lime-silica glass	2464.9	1.00730	898.61
Borosilicate glass	2124.9	1.14890	779.74
Organic glasses			
PMMA (poly(methyl ethacrylate))	1184.9	0.19120	1456.40
PC (polycarbonate)	1198.0	0.20512	1199.00
PDMS (polydimetylosiloxane)	965.0	0.15000	1460.00

2.4 Boundary conditions

Besides the side and bottom walls where constant room temperature of 24°C was applied, for the other walls Neumann boundary conditions were used. Due to the isolation at the top surface, adiabatic conditions were

implemented, covering the gold plate as well. Furthermore, the heat generation rate for the gold slab film was set with the Lambert–Beer–Bourger law assumption, yielding

$$S_e = \sigma_{abs_o} I_{abs} = \sigma_{abs_o}(1 - R_o) I_o \left[1 - \exp\left(-\sigma_{abs_o} \frac{l_{gold}}{\sqrt{1 - \dfrac{\sin\alpha}{n}}} \right) \right] \tag{6}$$

with the values (in room temperature) [33]:

$$\begin{aligned} R_o &= 0.705 \ \text{(for 532 nm)}, & I_o &= \eta \frac{P_L}{A} = 32000 \ \text{Wm}^{-2}, \\ P_L &= 0.8 \ \text{W}, & \eta &= 0.43, \\ n &= 0.55 \ \text{(for 532 nm)}, & \alpha &= 0^\circ, \qquad l_{gold} = 20 \ \text{nm}. \end{aligned}$$

Here, σ_{abs_o} may be expanded onto ξC_{ext}. The parameter ξ shall be concerned as an occupation of Au NPs in selected volume. They were assumed as separated from each other and embedded on the considered media (as inclusions). In this paper Au NPs are displaced with the high occupation factor 0.70, referring to the words "densely packed" in the title. It equals here about $\xi = 3 \times 10^{22}$ m^{-3}. Having substituted the appropriate values for 532 nm wavelength according to [14, 17], the σ_{abs_o} provides approximately 5.3×10^7 m^{-1}, and $S_e = 3.28 \times 10^{11}$ Wm^{-3} which corresponds circa 8.8% efficiency versus incident beam power [7, 11].

2.5 Calculation scheme

The conditions were reproduced in the simulations to reveal the temperature distributions into the glass. There were applied two parts: heating with a constant value of S_e and cooling where the value of heat generation rate S_e was set to zero. Each stage lasted for 120 s.

For the calculations, a second-order upwind algorithm with CFD code with the least squares cell based gradient evaluation was applied. Momentum and mass conservation equations, however, were converged but not calculated due to the presence of solids. Nevertheless, the approach might be expanded onto fluids as well, which may be done in reference to the fluid chamber. This approach could also be extended to liquids if the gold nanoparticles were plasticized. It is a theoretical possibility that so much thermal energy would enter the material that the gold would undergo a phase change from solid to liquid. Neither fluid nor Au NPs, however, underwent the plasticization because of the relatively low power of the selected laser. However, there has been presented such an extensive model in

order to include the possible gold phase transition and the slip at the walls where the Au NPs was embedded.

As a time regime, a bounded second order implicit scheme was used. The timestep was calculated and adjusted to 0.002 s in order to reduce the problem with conservation of energy during simulation. After each 250 timesteps (savestep) all energy and temperature changes in the bodies were being saved into a file for further analysis. All essential information about calculation has been presented in Table 3.

Table 3: General information of calculations parameters.

Parameter	Value
Heating time	120 s
Cooling time	120 s
Timestep	0.002 s
Savestep	0.5 s
Number of steps	60000
Iteration per one timestep	25
Mean CPU time	56 h = 201600 s

3 Results

The temperature distribution in terms of time was examined in order to investigate the temperature increase during all simulations. The reading data area has been established at the gold plate (5 mm × 5 mm at the top), Fig. 3.

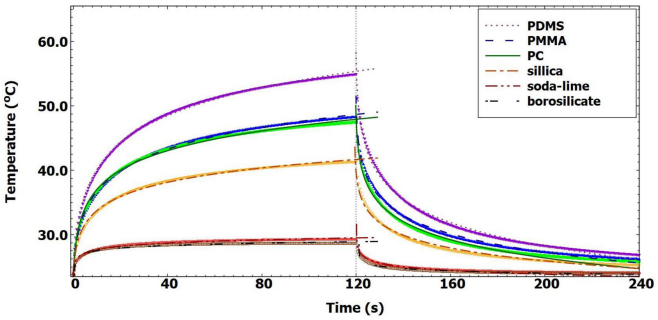

Figure 3: Mean temperature of the gold slab in terms of time for the studied materials presented in Table 2.

To study the heat transfer inside glasses, the temperature distribution as plots in three axes and temperature contours representation have been presented in Figs. 4–11, for materials presented in Table 2, respectively at particular 10, 120, and 150 s into the simulations.

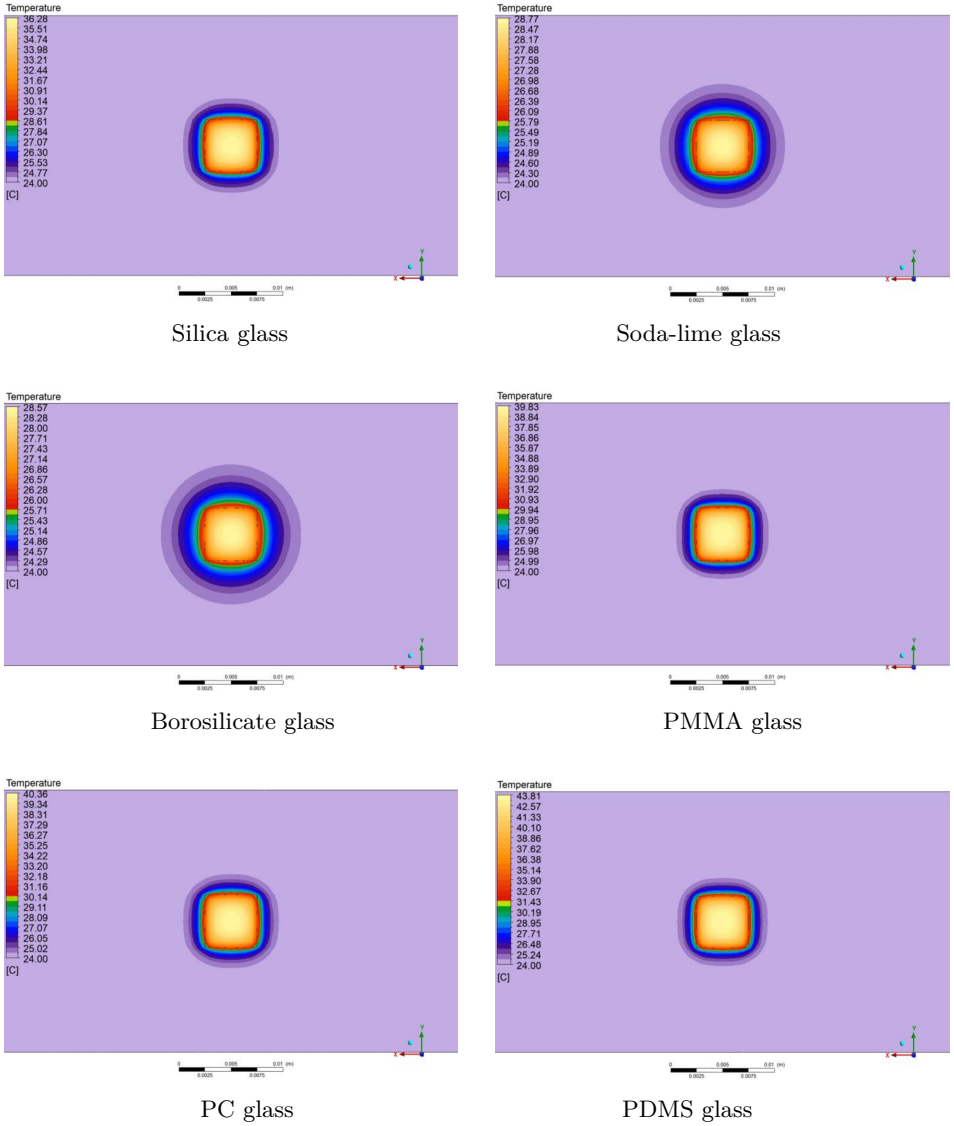

Figure 4: Temperature distribution after 10 s of irradiation at the top view of gold plate (XY-plane).

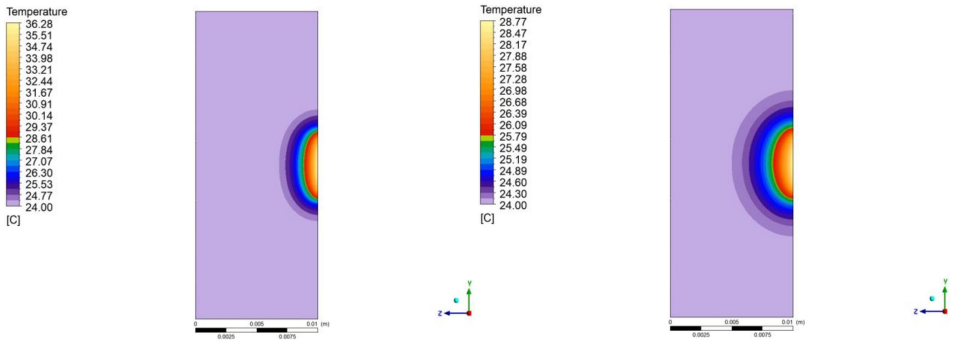

Silica glass Soda-lime glass

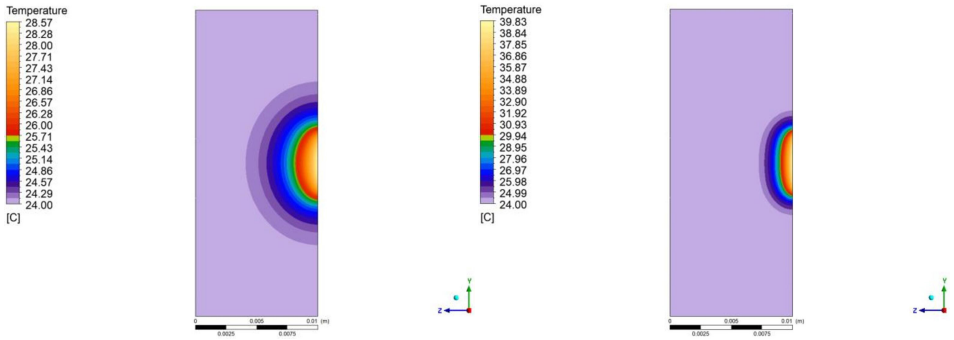

Borosilicate glass PMMA glass

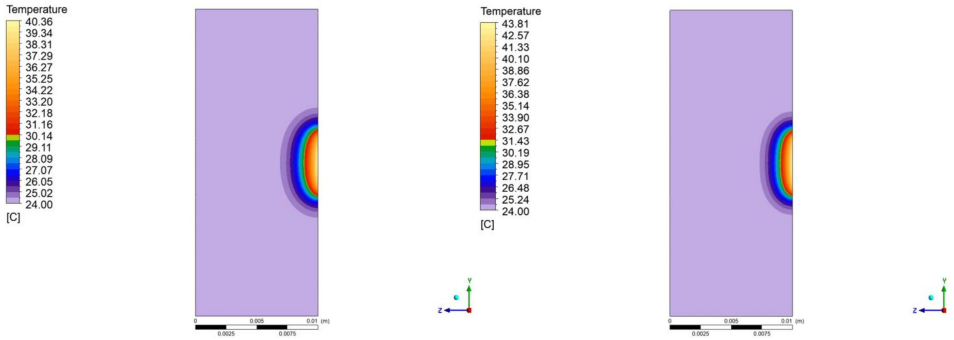

PC glass PDMS glass

Figure 5: Temperature distribution after 10 s of irradiation at view into a glass (XY-plane).

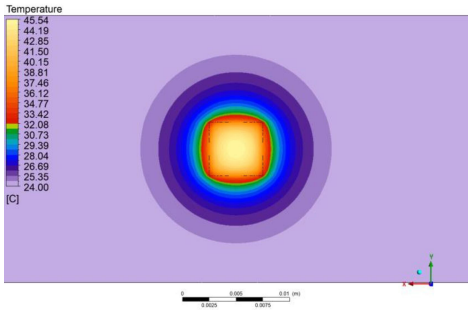

Silica glass

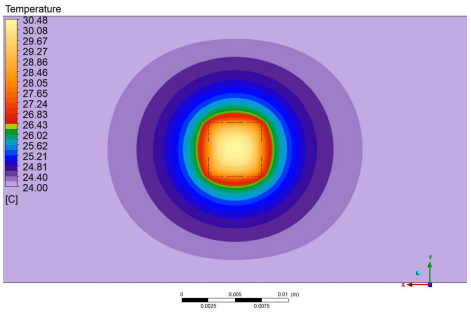

Soda-lime glass

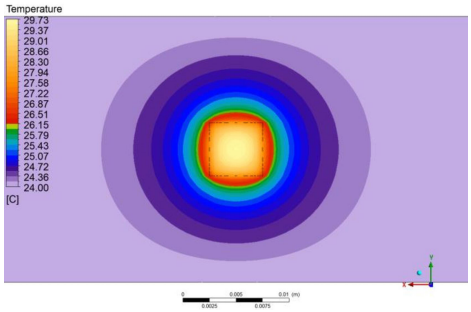

Borosilicate glass

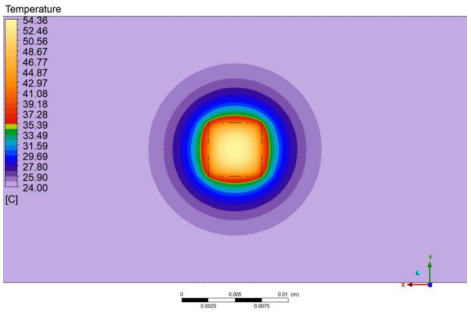

PMMA glass

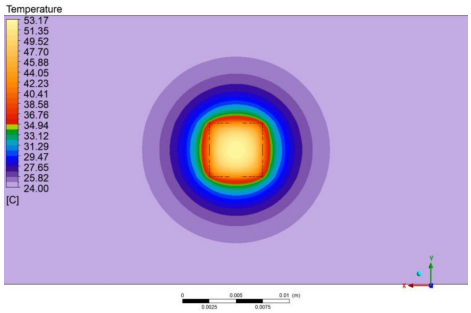

PC glass

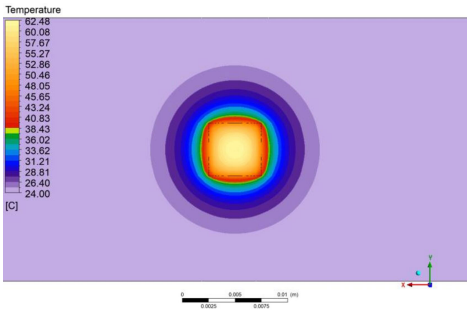

PDMS glass

Figure 6: Temperature distribution after 120 s of irradiation at the top view of gold plate (XY-plane).

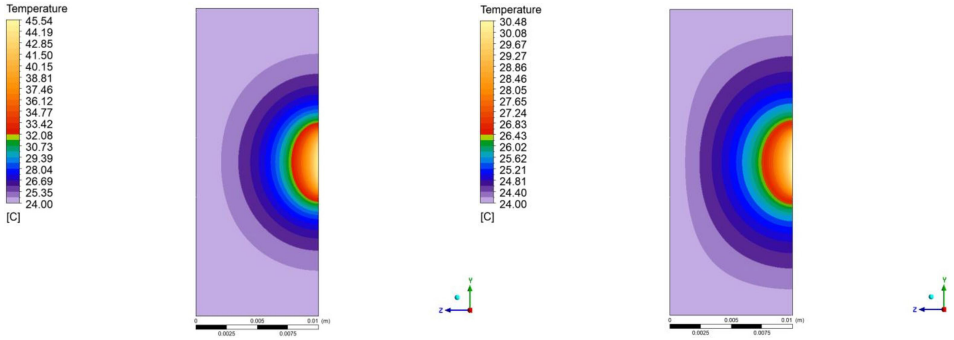

Silica glass Soda-lime glass

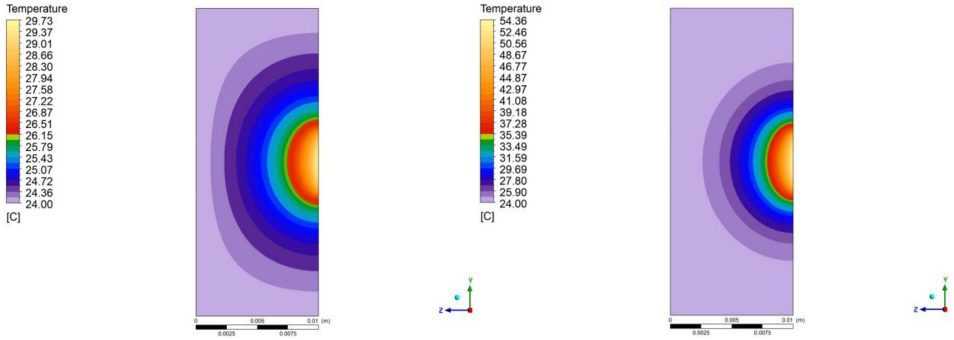

Borosilicate glass PMMA glass

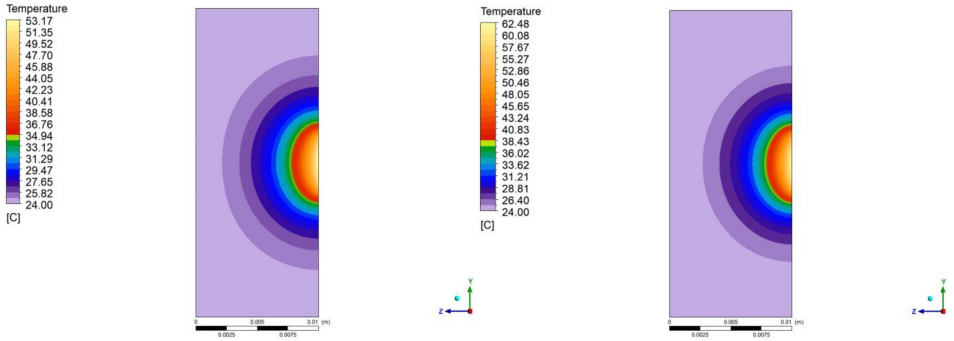

PC glass PDMS glass

Figure 7: Temperature distribution after120 s of irradiation at side view into a glass (XY-plane).

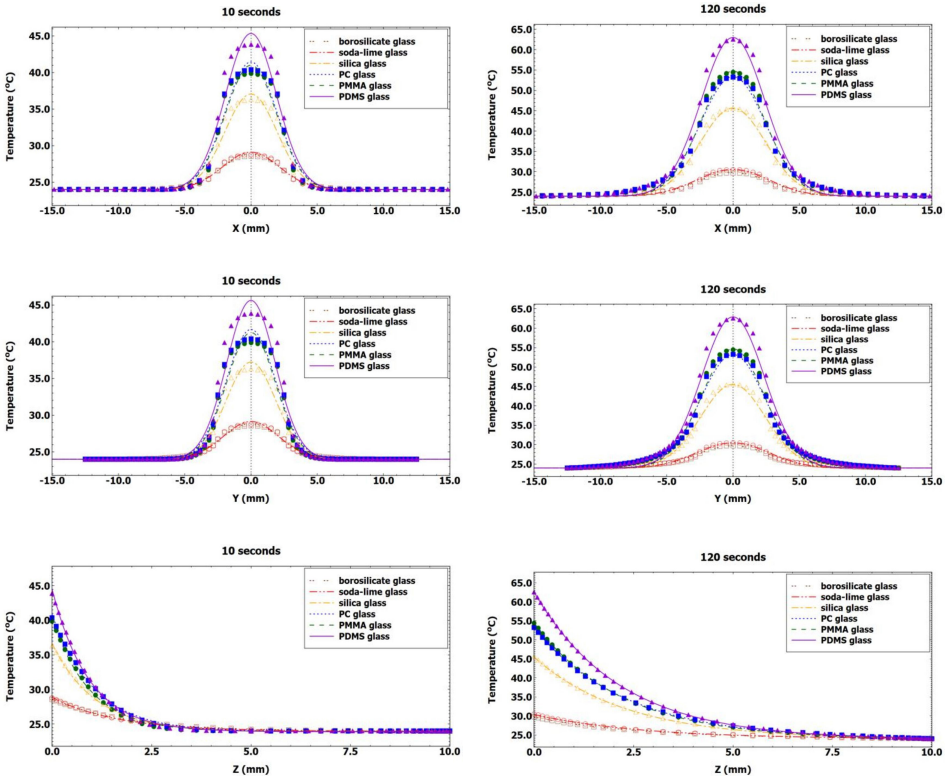

Figure 8: Plots of temperature distribution at a heating part.

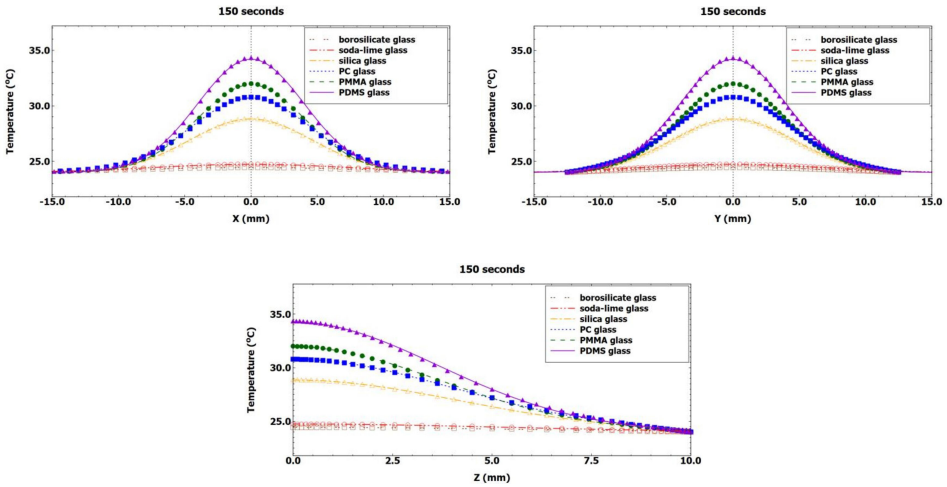

Figure 9: Plots of temperature distribution at cooling part.

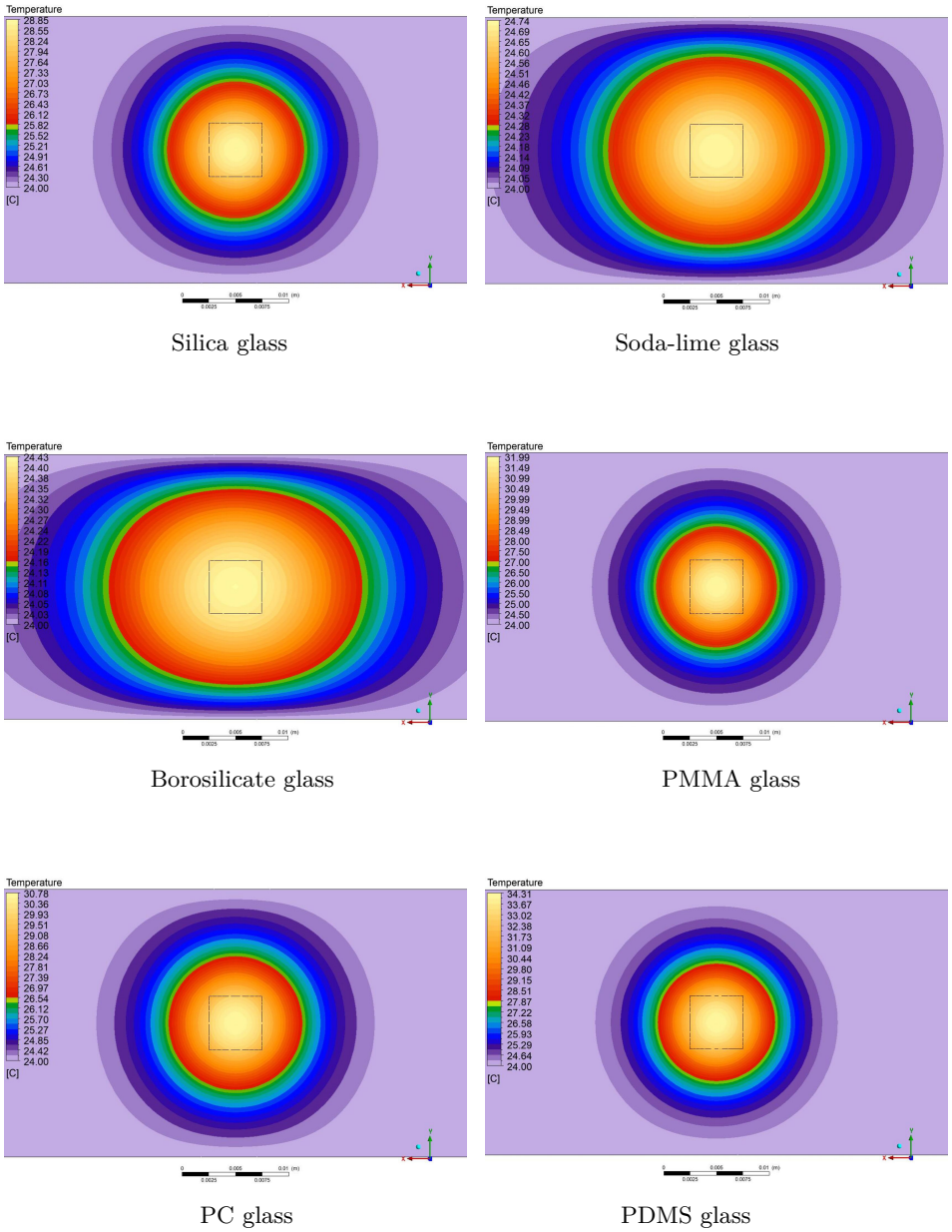

Silica glass | Soda-lime glass

Borosilicate glass | PMMA glass

PC glass | PDMS glass

Figure 10: Temperature distribution after 30 s of cooling (after the laser was turned off) at the top view of gold plate (XY-plane).

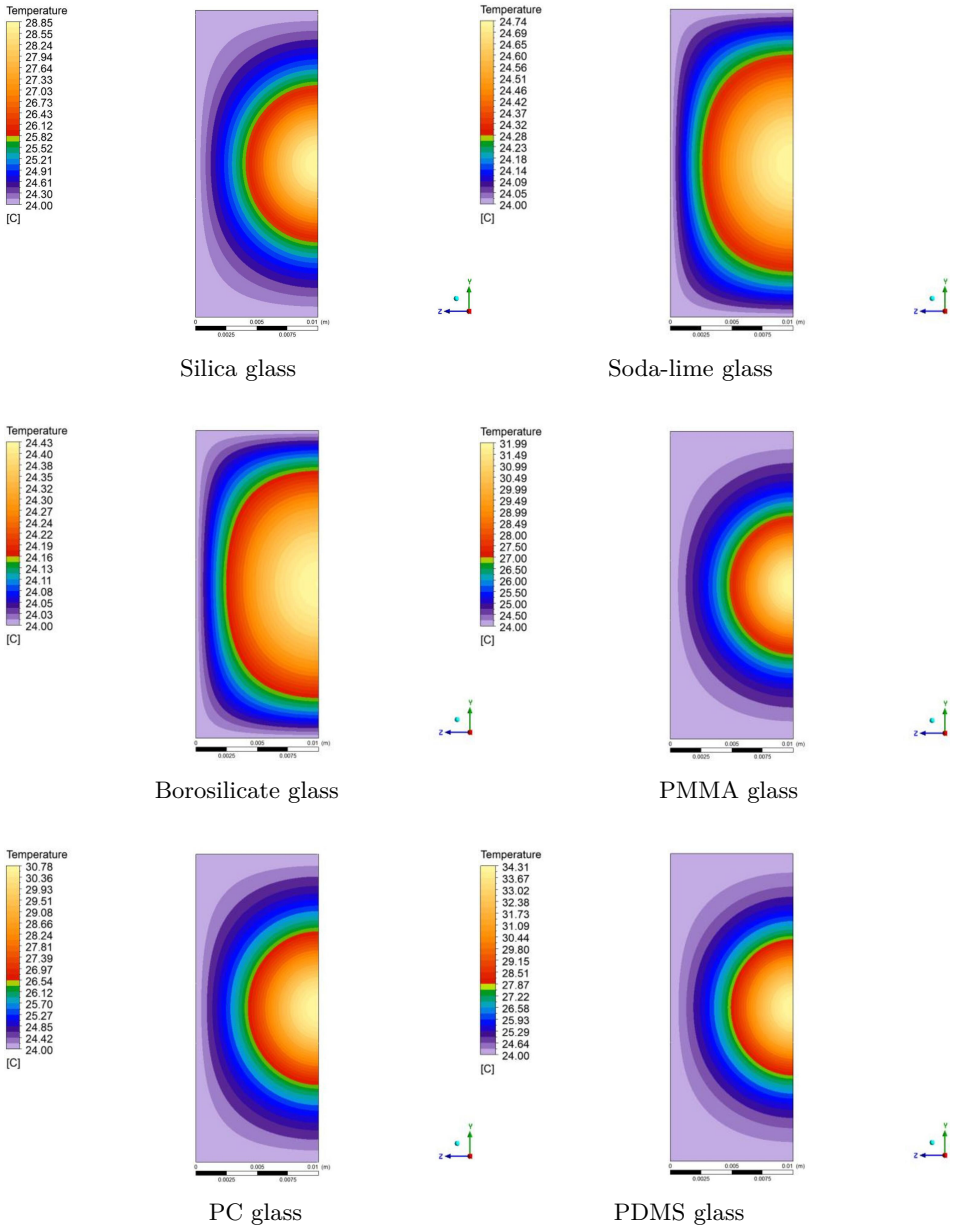

Figure 11: Temperature distribution 30 s of cooling (after the laser was turned off) at side view into a glass (XY-plane).

4 Discussion

Having compared all the figures, the obtained results correspond to the Newton's law of cooling what has been confirmed with an $y \sim a\exp(-bx)$ (where a and b are constant) dependence for all fitted curves. It stays for the argument that the validity of the results have been guaranteed. Noticeably, for the biological application, the temperature increase (and decrease as well) is most acute at the first 10 s of irradiation. After the time, the temperature changes much slower. Moreover, maximum temperatures are clearly dependent on the type of material and for the PDMS one reaches the highest 62.48°C after 120 s of irradiation while for the borosilicate glass this value equaled the lowest 29.73°C. As is depicted in Figs. 4–5, the same temperature is reached slightly earlier in some materials than in the other ones. Since thermal conductivity coefficient k may be considered as a sort of speed of heat transfer indicator, obviously the heat radius will be greater as well in the glasses with greater values of conductivity coefficient than the less, although the organic materials require using less energy to obtain higher values of temperature.

Hence, thermal conductivity coefficient k and the temperature difference between two cells ΔT shall be related to each other. It is connected mainly with the thermal conductivity coefficient and Fourier's law ($\vec{q} = k\,\mathrm{grad}\,T$). At the same depth they are inversely proportional regardless of the stage. These dependencies have been proved in Fig. 12, where the fitting curves ($T \sim k^{-1}$) stay in agreement with simulation results and all deviations might come from the measurement errors. Moreover, the fitted curves confirm the validity of the results have been guaranteed. However, they demonstrate the relationship only with thermal conductivity coefficient k, not with density and specific heat capacity of glasses even though their differences are significant. Nevertheless, heat transfer in selected media takes a typical behaviour and however, these results might undergo a severe change including the temperature and the size effects of the parameters.

It might be also noticed that temperature distributions at Z-axis assume the exponential shape $T(x) = T_{t_o}\exp(-ux)$ (where T_{t_o} and u are the temperature at initial stage, and constant) at the heating stage while after turning off the laser all dependence becomes a Gaussian curve. A similar behavior might be observed at Y- and Z- axes and it may be explained with the energy equation (1) and the heat generation rate. As the sample was being irradiated the temperature increased and the heat generation rate S_e had a constant value and at the cooling part this value was equal to zero

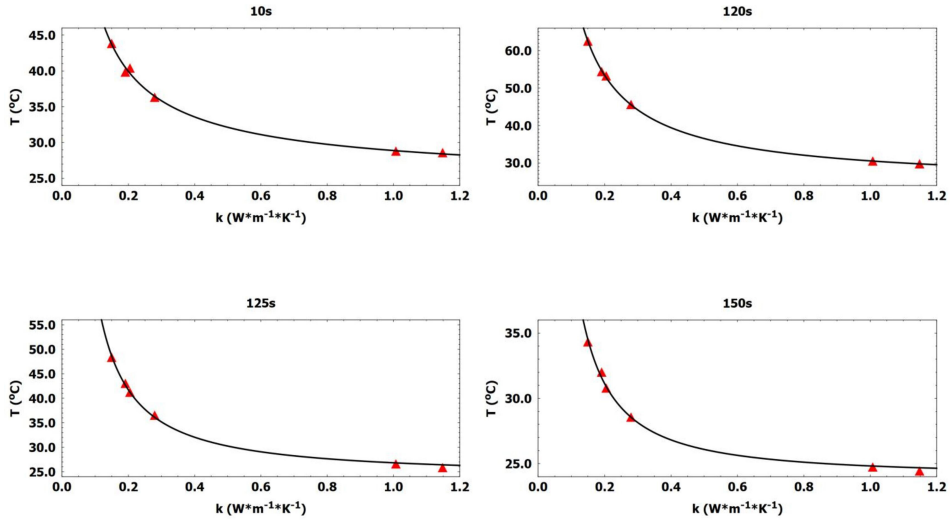

Figure 12: Maximum temperature values in the examining timesteps for the glasses in Table 2. The fitting curves have been fitted to the $y \sim x^{-1}$ function.

which simplified the equation formula to a Gaussian character. A similar approach might be applied in the Z-axis.

In reference to biological applications it is worth noticing that the 0.8 W laser power is sufficient for providing the temperature increase above a dozen Celsius degrees in less than two minutes. What is worth realizing is that it is necessary to adjust the laser power or geometry for the high-k materials in which a vast area undergoes heating. Whereas, like in the quartz glass or PDMS, the laser heated a narrower region, which admittedly provides greater temperature than 42°C, it requires much more time to cover the whole considered area. An increase of the laser power might deliver the same results taking a larger radius of sphere as at low-k values. Naturally, the selection of material depends also on the availability of materials, their price and accuracy of thermal camera, which might study the temperature distribution experimentally.

Nevertheless, it should be considered the real shape and location of gold nanoparticles, when they are placed freely in case the biological media. The assumption that the Au NPs are embedded on a plate is sort of premature. On the other hand, there have recently appeared many promising publications which suggested that the approach is getting gradually possible to be realized [38].

To summarize, soda-lime-silica glass and borosilicate glass give the possibility to cover a wide region of heating. Borosilicate glass provides the largest filling of the computational area with a reasonably temperature field, and it is intended to use these materials for further studies. Owing to the maximum heating area, the borosilicate or soda-lime glass, which is to serve as a base, should be selected for the future experiment.

5 Conclusions

There have been six simulations examined for the most used glasses and polymers in the industry and science. Heat generation appeared as a result of laser ablation of the gold plate consisting of densely packed gold nanoparticles. Having treated the Au NPs as a thin film and having specified the appropriate boundary conditions, the calculations have been run with the second-order upwind algorithm. After the simulations, the temperature changes inside glasses have allowed to take a look at which way the temperature changes, which is highly improbable to measure in the future experiment. Such an approach has allowed to specify the temperature distribution and heat transfer in terms of thermal conductivity of a glass.

Temperature contours have demonstrated the spherical distribution for all simulations. On the other hand, the temperature plots at X and Y-axes have shown the near-Gaussian and Gaussian distribution respectively at the heating and cooling stage because of the constant value of heat generation. The maximum temperature obtained after the irradiation was in the range 29.73–62.48°C depending on the thermal conductivity coefficient. This relationship has also been revealed based on Fourier law of conduction.

The results have also pointed out the gold nanoparticles in biological application would be the most effective in a similar-to-water-k-coefficient medium. In such a situation, the availability of materials, the heating area and the effectiveness of laser irradiation appear to lie at the optimum line. This condition provides either the soda-lime and borosilicate glass.

The study also revealed that the organic materials possessed lower values than inorganic ones due to much more irregular structure. At real systems, thermal conductivity coefficient k, specific heat capacity c_p, density ρ and heat generation rate S_e are all functions of temperature, which is highly observed in human tissues, and geometry of gold nanoparticles. Therefore, the temperature distributions would take slightly different dependencies. However, the sequence of the glasses with a maximum temperature should

remain unchanged for preliminary analysis. For more accrued analysis the glasses with similar-to-water-k-coefficient medium (like borosilicate glass) should be further considered.

Acknowledgements The first author of the paper is grateful to the Doctoral School at Gdańsk University of Technology for a scholarship which has allowed to study the presented topic.

Received 19 April 2021

References

[1] Dash S., Mohanty S., Pradhan S., Mishra B.K.: *CFD design of a microfluidic device for continuous dielectrophoretic separation of charged gold nanoparticles*. J. Taiwan Inst. Chem. Eng. **58**(2016), 39–48.

[2] Paruch M., Mochnacki B.: *Cattaneo-Vernotte bio-heat transfer equation. Identification of external heat flux and relaxation time in domain of heated skin tissue*. Comput. Assist. Meth. Eng. Sci. **25**(2018), 2–3, 71–80.

[3] Alia M.E., Sandeep N.: *Cattaneo-Christov model for radiative heat transfer of magnetohydrodynamic Casson-ferrofluid: A numerical study*. Results Phys. **7**(2017), 21–30.

[4] Paruch M., Majchrzak E.: *The modelling of heating a tissue subjected to external electromagnetic field*. Acta Bioeng. Biomech. **10**(2008), 2, 29–37.

[5] Feng B., Li Z., Zhang X.: *Prediction of size effect on thermal conductivity of nanoscale metallic films*. Thin Solid Films **517**(2009), 8, 2803–2807.

[6] Wang B.-X., Zhou L.-P., Peng X.-F.: *Surface and size effects on the specific heat capacity of nanoparticles*. Int. J. Thermophys. **1**(2006), 27, 139–151.

[7] Mie G.: *Beträge zur Optik trüber Medien, speziell kolloidaler Metalösungen*. Annalen der Physik **330**(1908), 3, 377–445.

[8] Pezzi L., De Sio L. Veltri I., Placido T. et al.: *Photo-thermal effects in gold nanoparticles dispersed in thermotropic menamic liquid crystals*. Phys. Chem. Chem. Phys. **17**(2015), 31, 20281–20287.

[9] Pierini F., Tabiryan N., Umeton C., Bunning T.J., De Sio L.: *Thermoplasmonics with Gold Nanoparticles: A new weapon in Modern Optics and Biomedicine*. Adv. Photonics Res. **2**(2021), 8, 1–17.

[10] Annesi F. et al.: *Biocompatible and biomimetic keratin capped Au nanoparticles enable the inactivation of mesophilic bacteria via photo-thermal therapy*. Colloid. Surface. A **625**(2021), 126950.

[11] Bohren C.F., Huffman D.R.: *Absorption and Scattering of Light by Small Particles*: Wiley-VCH, 1998.

[12] Guglielmelli A. et al.: *Biomimetic keratin gold nanoparticle-mediated in vitro photothermal therapy on glioblastoma multiforme*. Nanomedicine **16**(2021), 2, 121–138.

[13] Black S.E.: *Laser ablation: Effects and Applications*. Nova Science, New York 2011.

[14] Radhakrishnan A., Murugesan V.: *Calculation of the extinction cross section and lifetime of a gold nanoparticle using FDTD simulations*. AIP Conf. Proc. **1620**(2014), 52–57.

[15] Giannini V, Fernandez-Domínguez A.I., Heck S.C., Maier S.A.: *Plasmonic nanoantennas: fundamentals and their use in controlling the radiative properties of nanoemitters*. Chem. Rev. **111**(2011), 6, 3888 – 3912.

[16] Louis C., Pluchery O. (Eds.): *Gold Nanoparticles for Physics, Chemistry and Biology*. Imperial College, London 2012.

[17] Martin R.J.: *Mie scattering formulae for non-spherical particles*. J. Mod. Optic. **12**(1993), 40, 2467–2494

[18] Myers T.G.: *Why are the slip lengths so large in carbon nanotubes?* Microfluid. Nanofluid. **10**(2011), 1145–1145.

[19] Whitby M., Cagnon L., Thanou M., Quirke N.: *Enhanced fluid flow through nanoscale carbon pipes*. Nano Lett. **8**(2008), 9, 2632–2637.

[20] Maxwell J.C.: *On stresses in rarified gases arising from inequalities of temperature*. Philos. T. R. Soc. Lond. **170**(1879), 231–25.

[21] Ziółkowski P., Badur J.: *A theoretical, numerical and experimental verification of the Reynolds thermal transpiration law*. Int. J. Numer. Method H. **28**(2018), 1, 64–80.

[22] Ziółkowski P.: *Porous structures in aspects of transpirating cooling of oxycombustion chamber walls*. AIP Conf. Proc. **2077**(2019), 020065-1–020065-9.

[23] Badur J., Freidt M., Ziółkowski P.: *Neoclassical Navier–Stokes equations considering the Gyftopolous–Beretta exposition of thermodynamics*. Energies **13**(2020), 1656, 1–32.

[24] Mikielewicz D.: *Hydrodynamics and heat transfer in bubbly two-phase flows*. Int. J. Heat Mass Tran. **46**(2002), 2, 207–220.

[25] Muszyński T., Mikielewicz D.: *Comparison of heat transfer characteristics in surface cooling with boiling microjets of water, ethanol and HFE7100*. Appl. Therm. Eng. **93**(2016), 1403–1409.

[26] Badur J.: *Concept of Energy Evolution*. Wydawn. IMP PAN, Gdańsk 2009 (in Polish).

[27] Smoluchowski M.: *On conduction of heat by rarefied gases*. Phyl. Mag. **46**(1898), 192–206.

[28] Smoluchowski M.: *On conduction of heat in pulverized solids*. Pol. Ac. Art. Sci. **2**(1927), 1, 66–77.

[29] Docherty S.Y., Borg M.K., Lockerby D.A., Reese J.M.: *Multiscale simulation of heat transfer in a rarefied gas*. Int. J. Heat. Fluid. Fl. **50**(2014), 114–125.

[30] Stephenson D., Lockerby D.A., Borg M.K., Reese J.M.: *Multiscale simulation of nanofluidic networks of arbitrary complexity*. Microfluid. Nanofluid. **18**(2015), 5–6, 841–858.

[31] Lockerby D.A., Patronis A., Borg M.K., Reese J.M.: *Asynchronous coupling of hybrid models for efficient simulation of multiscale systems*. J. Comput. Phys. **284**(2015) 261–272.

[32] Sobieski W., Zhang Q.: *Multi-scale modeling of flow resistance in granular porous media*. Math. Comput. Simulat. **132**(2017), 159–171.

[33] Johnson P.B., Christy R.W.: *Optical constants of the noble metals*. Phys. Rev. B. **6**(1972), 12, 4370–4379.

[34] Narottam P.B.: *Handbook of Glass Properties*. Academic Press, New York 1986.

[35] Agari Y., Ueda A., Omura Y.: *Thermal diffusivity and conductivity of PMMA/PC blends*. Polymer **38**(1997), 4, 801–807.

[36] Cahill D.G., Olson J.R., Fischer H.E., Watson S.K., Stephens R.B., Tait R.H., Ashworth T., Pohl R.O.: *Thermal conductivity and specific heat of glass ceramics*. Phys. Rev. B **44**(1991), 22, 226–232,

[37] James E.M. (Ed.): *Polymer Data Handbook*. Oxford University Press (1999), 131, 363–367, 411–435, 655–657.

[38] Dixon M.C., Daniel T.A., Hieda M., Smilgies D.M., Chan M.C., Allara D.L.: *Preparation, structure, and optical properties of nanoporous gold thin films*. Langmuir **23**(2007), 5, 2414–2422.

[39] Harvey B.S.: *Hyperthermia*. New Engl. J. Med. **329**(1993), 483–487.

[40] Barichello L.B., Siewert C.E.: *A discrete-ordinates solution for a non-grey model withcomplete frequency redistribution*. J. Quant. Spectrosc. Ra. **2**(1999), 2, 665–675.

[41] Koniorczyk P., Zmywaczyk J.: *Analysis of thermal conductivity reduction in grey medium using a discrete ordinate method and the Henyey–Greenstein phase function for absorbing, emitting and anisotropically scattering media*. Arch. Thermodyn. **29**(2008), 2, 47–60.

[42] Filkoski R.V.: *Radiation heat transfer modeling and CFD analysis of pulverized-coal combustion with staged air introduction*. Arch. Thermodyn. **30**(2009), 4, 97–118.

[43] Dabrowski P.: *Selected studies of flow maldistribution in a minichannel plate heat exchanger*. Arch. Thermodyn. **38**(2017), 3, 135–148.